Supplement of Atmos. Meas. Tech., 17, 1617–1632, 2024
https://doi.org/10.5194/amt-17-1617-2024-supplement

Atmospheric Measurement Techniques
Open Access
EGU

Supplement of

Verification of parameterizations for clear sky downwelling longwave irradiance in the Arctic

Giandomenico Pace et al.

Correspondence to: Giandomenico Pace (giandomenico.pace@enea.it)

Table S1: Statistical indices for the different formulas (see table 1) with the original coefficients applied to THAAO data from 2017; the best performances of the main statistical indices are highlighted in bold.

Formula number	Bias (W/m2)	Standard difference (W/m2)	R^2	Slope	Skewness of the differences	Kurtosis of the differences	KGE	T_Skill	5^{th} percentile	25^{th} percentile	50^{th} percentile	75^{th} percentile	95^{th} percentile	RMSE (W/m2)
1	29.1	8.0	0.964	0.925	-0.207	0.751	0.834	0.962	15.71	23.67	29.08	34.65	42.08	30.16
2	17.8	9.0	0.971	1.098	0.176	1.051	0.851	0.960	4.56	11.5	17.31	23.35	33.46	19.93
3	-5.6	12.0	0.962	1.165	0.670	0.844	0.804	0.933	-21.19	-14.32	-7.28	1.11	17.89	13.26
4	26.1	14.2	0.938	0.676	-0.102	-0.997	0.701	0.857	3.46	14.22	26.92	38.01	47.11	29.75
5	8.1	8.2	0.964	**1.001**	0.061	1.250	0.947	0.963	-4.96	3.02	7.52	13.2	22.01	11.5
6	-18.5	13.1	0.975	1.238	0.279	-0.236	0.725	0.926	-37.2	-28.42	-20.45	-8.98	3.91	22.66
7	1.7	9.8	0.965	0.823	-0.304	-0.307	0.840	0.937	-14.84	-5.43	2.56	8.91	16.68	9.95
8	16.2	7.5	0.971	1.030	-0.182	1.591	0.902	0.970	3.87	11.53	16.09	21.05	28.35	17.88
9	-10.9	7.5	0.972	0.911	-0.246	0.449	0.903	0.966	-23.53	-15.92	-10.7	-5.67	1.35	13.22
10	-51.7	10.9	0.973	0.772	-0.212	-0.743	0.648	0.917	-69.71	-60.14	-51.04	-42.82	-35.14	52.85
11	3.9	7.2	0.972	0.925	-0.321	0.578	0.940	0.969	-8.75	-0.77	4.2	9.04	15.09	8.23
12	5.9	6.6	0.974	0.971	-0.288	2.622	0.963	0.974	-4.94	1.79	5.69	10.09	16.73	8.83
13	39.8	47.5	0.924	1.989	-0.336	-0.317	-0.104	0.564	-37.48	4.98	47.39	73.39	112.9	61.98
14	47.1	44.1	0.924	1.907	-0.358	-0.256	-0.028	0.593	-24.96	15.04	53.99	77.94	114.95	64.48
15	18.8	11.4	0.924	0.889	-0.338	0.675	0.872	0.920	-0.84	11.74	18.74	26.83	37.14	21.95
16	**0.9**	6.9	0.982	0.874	-0.375	0.870	0.891	0.969	-10.41	-4.18	**1.19**	6.13	11.36	6.91
17	**0.9**	**5.8**	**0.984**	0.912	-0.671	3.483	**0.930**	**0.979**	-8.67	-3.15	1.35	5.03	9.7	**5.9**

Table S2: Statistical indices for the different formulas (see table 1) with the original coefficients applied to THAAO data from 2018; the best performances of the main statistical indices are highlighted in bold.

Formula number	Bias (W/m2)	Standard difference (W/m2)	R^2	Slope	Skewness of the differences	Kurtosis of the differences	KGE	T_Skill	5^{th} percentile	25^{th} percentile	50^{th} percentile	75^{th} percentile	95^{th} percentile	RMSE (W/m2)
1	29.7	7.1	0.970	0.922	-0.451	2.180	0.822	0.967	18.55	25.24	29.66	34.26	41.00	30.49
2	16.9	8.2	0.974	1.107	-0.142	1.291	0.849	0.963	5.20	11.02	16.67	22.67	30.32	18.82
3	-7.1	10.7	0.968	1.150	0.707	1.969	0.809	0.941	-20.49	-14.42	-8.97	-1.08	11.61	12.85
4	28.9	13.3	0.949	0.672	-0.261	-0.588	0.683	0.860	6.54	19.54	29.18	39.37	49.24	31.78
5	8.0	7.0	0.970	**0.993**	-0.286	2.921	0.949	0.970	-2.48	3.53	7.94	12.43	19.63	10.67
6	-21.1	13.2	0.974	1.267	0.419	-0.659	0.700	0.919	-37.11	-31.24	-24.81	-9.57	1.54	24.84
7	3.2	9.0	0.971	0.820	-0.448	0.325	0.835	0.941	-12.07	-2.33	3.70	9.88	16.74	9.55
8	16.1	6.7	0.975	1.039	-0.658	2.750	0.897	0.973	5.65	11.43	16.60	20.91	26.14	17.47
9	-10.0	6.7	0.975	0.923	-0.382	2.018	0.909	0.970	-20.45	-14.39	-10.24	-5.34	1.08	12.02
10	-49.9	10.1	0.975	0.783	-0.395	-0.222	0.648	0.923	-67.20	-56.62	-49.19	-42.22	-34.80	50.89
11	4.1	7.0	0.969	0.959	-0.589	1.066	0.958	0.968	-7.89	-0.46	4.73	9.19	14.55	8.14
12	6.6	5.6	0.980	0.972	-0.950	7.183	**0.959**	0.980	-1.49	3.08	6.51	10.20	15.50	8.69
13	39.1	45.8	0.910	1.984	-0.309	0.399	-0.094	0.559	-35.30	9.76	37.26	74.23	110.00	60.24
14	46.6	42.6	0.910	1.902	-0.351	0.513	-0.020	0.588	-22.83	19.79	45.43	78.98	112.37	63.15
15	22.3	11.9	0.910	0.887	-1.145	2.505	0.848	0.906	-0.67	16.41	24.12	30.48	37.46	25.25
16	2.8	6.2	0.985	0.886	-0.920	4.687	0.893	0.973	-6.81	-0.85	2.57	7.25	12.24	6.80
17	**2.4**	**5.1**	**0.987**	0.925	-1.290	10.662	0.931	**0.982**	-4.96	-0.79	**2.19**	5.98	10.28	**5.66**

Table S3: Statistical indices for the different formulas (see table 1) with the coefficients derived from the THAAO data for 2017; the best performances of the main statistical indices are highlighted in bold.

Formula number	Bias (W/m2)	Standard difference (W/m2)	R^2	Slope	Skewness of the differences	Kurtosis of the differences	KGE	T_Skill	5^{th} percentile	25^{th} percentile	50^{th} percentile	75^{th} percentile	95^{th} percentile	RMSE (W/m2)
1	-1.26	10.61	0.964	0.794	-0.335	-0.432	0.812	0.924	-19.3	-8.99	-0.27	6.75	14.65	10.68
2	0.14	7.23	0.970	0.985	-0.256	1.390	0.985	0.970	-12.34	-4.29	**0**	4.94	11.88	7.24
3	0.93	13.42	0.962	1.206	0.699	0.610	0.763	0.921	-16.08	-9.03	-1.3	8.33	27.19	13.45
4	0.02	8.48	0.961	0.915	-0.145	0.840	0.933	0.957	-13.67	-5.54	**0**	5.72	13.93	8.48
5	-0.03	7.96	0.964	0.959	-0.117	0.974	0.973	0.964	-13.31	-5.07	-0.41	5.35	13.19	7.96
6	0.88	18.55	0.975	1.381	0.378	-0.702	0.599	0.872	-24.77	-13.9	-3.05	15.38	32.74	18.57
7	**0.00**	7.58	0.971	1.030	-0.107	1.637	0.949	0.969	-11.99	-5.08	-0.09	4.76	12.79	7.58
8	-0.01	7.04	0.972	0.986	-0.344	1.509	0.986	0.972	-12.35	-4.35	**0**	4.71	11	7.04
10	-5.38	7.10	0.971	0.968	-0.265	1.463	0.964	0.971	-17.54	-9.75	-5.58	-0.61	6.21	8.91
11	0.01	6.58	0.975	0.974	-0.454	1.895	0.984	0.975	-11.26	-4.13	0.3	4.35	10.17	6.58
12	0.25	5.95	0.980	**0.999**	-0.455	6.606	0.978	0.980	-8.72	-3.2	0.02	3.46	10.46	5.96
14	-0.09	11.32	0.924	0.928	-0.361	0.993	0.952	0.924	-18.8	-7.03	**0**	7.62	18.33	11.33
16	0.18	5.40	0.983	0.977	-0.759	7.358	**0.991**	0.983	-8.68	-3.06	0.4	3.48	8.28	5.4
17	**0.00**	**5.21**	**0.984**	0.972	-0.982	8.785	0.989	**0.984**	-8.66	-3.06	0.29	3.35	7.52	**5.21**

Table S4: Statistical indices for the different formulas (see table 1) with the coefficients derived from the THAAO data for 2018; the best performances of the main statistical indices are highlighted in bold.

Formula number	Bias (W/m2)	Standard difference (W/m2)	R^2	Slope	Skewness of the differences	Kurtosis of the differences	KGE	T_Skill	5th percentile	25th percentile	50th percentile	75th percentile	95th percentile	RMSE (W/m2)
1	-1.18	10.03	0.970	0.784	-0.514	0.040	0.801	0.924	-18.9	-7.5	-0.3	6.4	13.3	10.1
2	-0.22	6.38	0.974	0.982	-0.630	3.178	0.985	0.974	-10.2	-4.4	0.0	4.1	9.6	6.38
3	0.83	12.44	0.968	1.204	0.835	1.537	0.758	0.925	-14.1	-7.8	-2.2	8.3	23.1	12.47
4	0.22	7.48	0.965	0.941	-0.241	2.144	0.953	0.964	-11.3	-4.1	**0.0**	4.8	12.4	7.48
5	-0.08	6.92	0.970	0.950	-0.416	2.604	0.969	0.969	-10.6	-4.5	-0.1	4.4	11.1	6.92
6	0.68	19.62	0.974	1.444	0.664	-0.831	0.547	0.850	-20.5	-14.5	-7.8	18.4	35.8	19.63
7	0.01	7.14	0.975	1.060	-0.403	2.080	0.928	0.970	-10.6	-4.9	0.2	4.8	11.4	7.14
8	-0.24	6.32	0.975	0.975	-0.666	3.144	0.977	0.974	-10.2	-4.4	**0.0**	4.0	9.4	6.33
10	-5.46	6.33	0.975	0.971	-0.585	3.066	0.962	0.974	-15.2	-9.5	-5.3	-1.2	4.4	8.36
11	0.09	6.95	0.970	0.985	-0.588	1.043	0.984	0.970	-11.2	-4.6	1.0	5.2	10.0	6.96
12	0.18	5.17	0.983	**1.003**	-1.385	11.710	0.984	0.983	-7.0	-2.7	0.1	3.1	8.2	5.17
14	-2.02	11.89	0.910	0.932	-1.211	3.126	0.946	0.911	-23.7	-8.1	**0.0**	6.1	13.1	12.06
16	0.14	4.68	0.986	0.985	-2.090	18.156	**0.991**	0.986	-6.7	-2.6	0.4	3.2	6.6	4.68
17	**0.00**	**4.51**	**0.987**	0.985	-2.331	21.330	**0.991**	**0.987**	-6.6	-2.5	0.2	2.8	6.2	**4.51**

Table S5: Statistical indices for the different formulas (see table 1) with the coefficients derived from the THAAO data for 2018; the statistical indices are calculated with respect to data for 2017. The best performances of the main statistical indices are highlighted in bold.

Formula number	Bias (W/m2)	Standard difference (W/m2)	R^2	Slope	Skewness of the differences	Kurtosis of the differences	KGE	T_Skill	5^{th} percentile	25^{th} percentile	50^{th} percentile	75^{th} percentile	95^{th} percentile	RMSE (W/m2)
1	-3.00	10.82	0.964	0.787	-0.335	-0.474	0.804	0.921	-21.41	-10.92	-2.00	5.25	13.16	11.23
2	-0.44	7.22	0.970	0.975	-0.270	1.300	0.982	0.970	-12.98	-4.87	-0.55	4.41	11.22	7.24
3	2.87	13.85	0.962	1.219	0.703	0.545	0.750	0.916	-14.62	-7.44	0.48	10.52	29.98	14.14
4	-0.25	8.49	0.959	0.938	-0.071	0.985	0.957	0.958	-13.34	-6.15	-0.44	5.48	13.87	8.50
5	-0.39	7.96	0.964	0.957	-0.124	0.958	0.972	0.964	-13.67	-5.45	-0.74	5.00	12.82	7.97
6	4.81	19.71	0.975	1.410	0.386	-0.752	0.568	0.860	-22.29	-11.04	0.58	20.31	38.67	20.29
7	0.71	7.83	0.971	1.047	-0.062	1.539	0.933	0.968	-11.42	-4.61	0.67	5.59	14.11	7.86
8	-0.72	7.06	0.972	0.963	-0.335	1.267	0.971	0.971	-13.05	-5.09	-0.66	4.09	10.53	7.09
10	-5.62	7.13	0.971	0.961	-0.270	1.365	0.960	0.971	-17.85	-10.05	-5.76	-0.77	5.94	9.07
11	**0.24**	6.67	0.975	0.951	-0.386	1.595	0.967	0.974	-10.95	-4.10	**0.43**	4.81	10.69	6.67
12	-0.46	5.93	0.980	**0.997**	-0.482	6.836	0.980	0.980	-9.38	-3.89	-0.68	2.74	9.74	5.95
13	-5.35	11.34	0.924	0.934	-0.367	1.041	0.947	0.925	-24.01	-12.30	-5.24	2.37	13.12	12.53
16	-1.04	5.39	0.983	0.972	-0.780	7.124	**0.987**	0.983	-9.93	-4.32	-0.76	2.29	7.00	5.49
17	-1.19	**5.23**	**0.984**	0.971	-0.952	8.561	0.986	**0.984**	-9.84	-4.32	-0.92	2.09	6.42	**5.36**

Table S6: Statistical indices for the different formulas (see table 1) with the coefficients derived from the THAAO data for 2017; the statistical indices are calculated with respect to data for 2018. The best performances of the main statistical indices are highlighted in bold.

Formula number	Bias (W/m2)	Standard difference (W/m2)	R^2	Slope	Skewness of the differences	Kurtosis of the differences	KGE	T_Skill	5^{th} percentile	25^{th} percentile	50^{th} percentile	75^{th} percentile	95^{th} percentile	RMSE (W/m2)
1	0.49	9.81	0.970	0.792	-0.508	0.100	0.808	0.928	-16.78	-5.65	1.33	7.87	14.77	9.82
2	**0.26**	6.40	0.974	0.992	-0.652	3.197	0.987	0.974	-9.72	-3.96	0.60	4.59	9.99	6.41
3	-1.00	12.03	0.968	1.191	0.811	1.628	0.771	0.929	-15.53	-9.29	-3.72	6.08	20.44	12.07
4	0.71	7.53	0.967	0.916	-0.350	1.876	0.928	0.962	-11.36	-3.59	0.76	5.38	12.74	7.56
5	0.26	6.92	0.970	0.951	-0.413	2.629	0.971	0.969	-10.20	-4.19	0.26	4.70	11.47	6.92
6	-2.99	18.50	0.974	1.414	0.640	-0.821	0.576	0.862	-23.24	-17.24	-10.67	13.88	30.00	18.74
7	-0.54	6.85	0.975	1.042	-0.482	2.491	0.945	0.972	-10.88	-5.17	**-0.23**	4.03	10.12	6.87
8	0.28	6.39	0.975	**0.999**	-0.749	3.100	0.986	0.975	-9.75	-4.03	0.79	4.76	9.68	6.39
10	-5.30	6.32	0.975	0.979	-0.603	3.136	0.966	0.975	-15.03	-9.31	-5.13	-1.09	4.53	8.25
11	-0.28	6.88	0.971	1.004	-0.650	1.196	0.980	0.971	-11.63	-4.91	0.65	4.86	9.39	6.89
12	0.87	5.18	0.983	1.005	-1.383	11.652	0.982	0.983	-6.31	-2.03	0.86	3.84	8.94	5.25
13	3.26	11.87	0.910	0.926	-1.202	3.043	0.940	0.910	-18.55	-2.72	5.22	11.34	18.40	12.31
16	1.33	4.69	0.986	0.990	-2.105	18.295	**0.990**	0.986	-5.55	-1.38	1.60	4.34	7.70	4.87
17	1.25	**4.53**	**0.987**	0.985	-2.355	21.451	0.989	**0.987**	-5.54	-1.21	1.48	4.10	7.35	**4.70**

SEASONAL VARIABILITY OF CLOUD-FREE OCCURRENCE AND PERFORMANCE OF THE ANNUAL PARAMETERIZATIONS FOR JANUARY-FEBRUARY AND JULY-AUGUST OF 2017-2018.

Figure S1 shows the monthly availability of the data necessary to carry out the study calculated using the number of minutes contained in each month. Even in the months with more data, the coverage does not exceed 85% mainly due to the measurements of the microwave radiometer that has scheduled interruptions of the IWV measurements to carry out internal calibrations and measurements at different zenith angles necessary to estimate the temperature profile.
As can also be deduced from the time series shown in Figure 1 of the manuscript, the periods with the greatest interruptions concern November and December 2017, caused by the missing of data first of the IWV and then of DLI and IBT, and of September 2018 due to the lack of DLI and IBT data, which are acquired by the same datalogger. In January and December 2017 there is a reduced percentage of observations also due to the snowfall accumulation on the pyrometer or pyrgeometer or both (see paragraph 4.2 *Clear sky screening procedure* of the manuscript), which was manually assessed by looking at the data.

The occurrence of cases of clear skies was evaluated both with respect to the total number of minutes present in each month and with respect to the performed measurements; they are called *monthly clear sky* and *normalized monthly clear sky*, respectively.
Using the *normalized monthly clear sky* (discussed in the present work), the strongest annual variations in the clear sky occurrence in the two years are found in April and June-July, months that in both 2017 and 2018 have presented a high number of observations.
The difference observed between April 2017 and 2018 constitutes an anomaly compared to the clear sky occurrence observed in March and June, which are substantially the same in the two years.

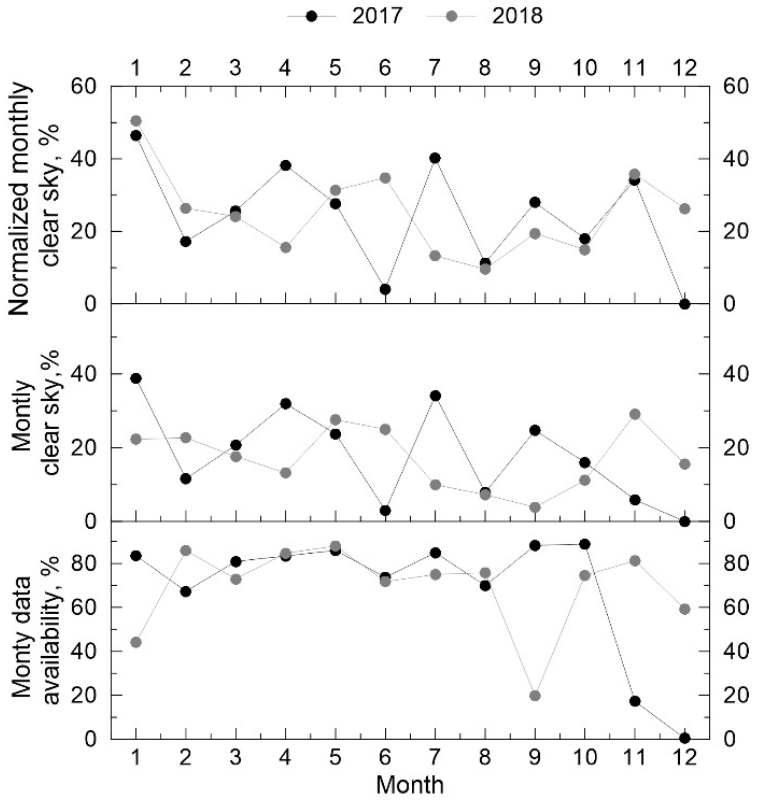

Figure S1. From bottom to top: time series of monthly data availability, of the monthly occurrence of clear skies calculated considering all the measurable data and of the normalized monthly occurrence of clear skies calculated with respect to the data measured.

The situation is different for the differences shown between June-July 2017 and 2018. In fact, the lower value of the clear sky in June 2017 compared to that of 2018, is compensated by the higher value in July 2017 compared to that of 2018, suggesting a different temporal development of the summer season.
For the remaining months, the *normalized monthly clear sky* is very similar for the two considered years.
Overall, both the monthly availability of the data used and the actual occurrence of clear skies during the two years are homogenous in relation to the variability of the parameters in Figure 3 of the manuscript, showing that the results are affected by reduced monthly representativeness of the measures.

As suggested by the reviewer, the effectiveness of the parameterizations optimized in 2017 and 2018 was tested for different periods of the year. Based on data temporal representativeness, we have chosen to verify the performances by grouping the months of January-February and July-August representative of the winter and summer periods, respectively. To present the results of the annual parameterization applied to different periods of the year, we show the bias and the RMSE values separately, reporting in Figure S2 the performances evaluated on the whole year, on the winter and summer periods, for both 2017 and 2018.
Some particularly high RMSE values (corresponding to parameterizations of ID#3, Swinbank (1963), and ID#6, Brutsaert (1975), in 2017 and of ID#6 in 2018), or bias values very far from 0 (ID#1, i.e. Maykut and Church (1973), ID#3 and ID#6 in both 2017 and 2018), do not appear in Figure S2 because they are very high and representative of parameterizations with low performance as already highlighted in the text of the manuscript. This choice was made to highlight the better performance of the other parameterizations.

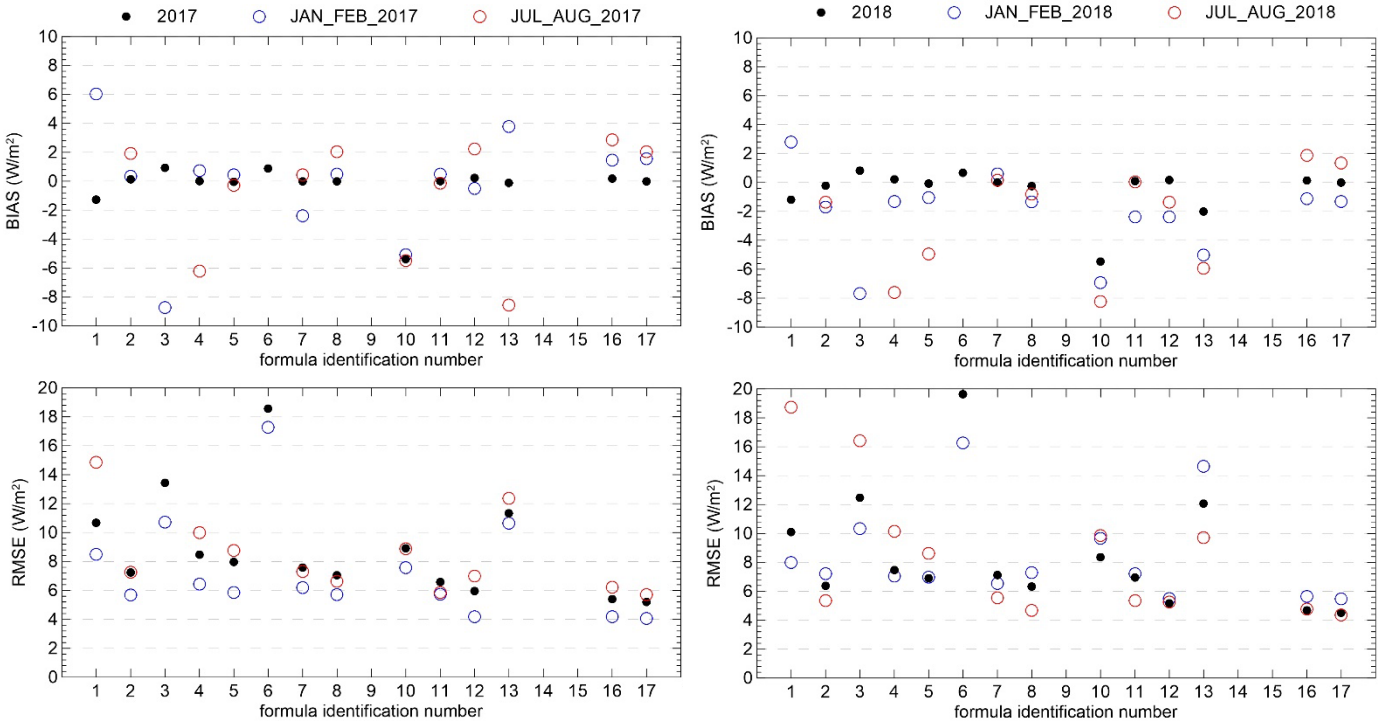

Figure S2. From bottom to top: on the left the values of RMSE and bias for the annual (black dot), winter (blue circle) and summer (red circle) data of 2017; on the right, the same for 2018. The performances were evaluated against the optimized parameterizations on annual data from 2017 and 2018 respectively. Some values of the RMSE of the parameterizations ID#3 (Swinbank, 1973), ID#6 (Brutsaert, 1975) in 2017 and of ID#6 in 2018, as well as some values of the bias of ID#1 (Maykut and Church, 1973), ID#3 and ID#6 in both 2017 and 2018, are out of scale of the plot (see comment in the text).

In terms of bias, considering both the seasonal differences of 2017 and 2018, no single parameterization always presents the best performance. In 2017 both ID#5, Ohmura (1981), and ID#11, Jin et al. (2006), show very small summer and winter values close to the annual ones. On the other hand, in 2018, ID#7, Satterlund (1979), shows this behavior, while ID#11 shows practically zero summer and annual bias, but a winter bias slightly larger than 2 W/m^2. The parameterizations of ID#12, Prata (1996), ID#13, Dilley and O'Brien (1998), and ID#14, Dilley and O'Brien (1998), have annual bias very close to 0 and present respectively positive and negative biases in the summer and winter seasons

(ID#12 in 2017, and ID #16 and ID#17 in 2018), or only negative for ID#12 in 2018 or only positive for ID#16 and ID#17 in 2018.
Regarding the seasonal bias, there is no homogeneous behavior between the parameterizations.

Considering the RMSE, in 2017, there is a behavior shared by practically all stations: the winter RMSE values are lower than the annual ones, and the summer ones are approximately equal to or slightly higher than the annual ones. It is interesting to note that in 2018 the RMSE values do not present this feature, for various parameterizations (ID#2, ID#7, ID#8, i.e. Idso (1981) and Andreas and Ackley (1994), ID#11, ID#12, ID#16 and ID#17) the summer value being less than or equal to the annual one.
The parameterizations ID#11, specifically developed for the Arctic and using both the values of e_s and T_s, ID#12, ID#16 and ID#17, generally show the lowest values of RMSE. Although the ID#12, ID#16 and ID#17 parameterizations use the values of e_s, T_s and IWV, it is notable that having been formulated for a global application, obtain these good results when applied to the peculiar conditions of the arctic region.
However also parametrizations ID#2, ID#7, and ID#8, show very good performance using respectively only e_s, ID#2, or e_s and T_s (ID#7 and ID#8).
The best performances are maintained around RMSE values between 4 and 6 W/m^2 and, therefore, are statistically comparable with the accuracy of the pyrgeometer measurement.

In conclusion, we highlight that the RMSE is calculated as the quadratic sum of the bias and the standard deviation (see paragraph 4.2 *Statistical indices* of the manuscript), therefore parameterizations that present a non-negligible bias (e.g. ID#16 and ID #17) and low RMSE have a lower standard deviation, indicating the ability to better follow the variability of the measurements, compared to the parameterizations showing a lower bias, but higher RMSE values.

The choice to use the pyrometer instead of the pyrgeometer itself to determine clear sky conditions, presents the advantage of a larger sensitivity to the presence of thin clouds, but the disadvantage of a reduced portion of sky detected at the zenith; this is the main factor that makes it difficult to associate a quantitative accuracy to the developed clear-sky detection method.
Simulations of the pyrometer zenith brightness temperature (IBT) and of the DLI have been carried out using the MODTRAN5.3 radiative transfer model (Berk et al., 2006), to evaluate the uncertainty associated with the presence of thin cirrus clouds. The aim was not only to verify the sensitivity of the pyrometer to the presence of cirrus, but also to quantitatively determine the influence of these clouds on the DLI.

The main characteristics of the simulations are summarized in the following table.

Atmopheric profile	Subarctic winter	Subarctic summer
IWV	0.3 cm	1.2 cm and 1.5 cm
Acloud base altitude	8 km	8 km
cloud base temperature	220.6 K	239.2 K
Geometrical depth	1 km	1 km
Cloud type	cirrus	cirrus

The MODTRAN internal cirrus model, called cirrus standard model, is based on ice particles with 64 μm effective radius. Overcast conditions are assumed. The cirrus optical thickness values have been of respectively 0.03, 0.1, 0.3, 1, 2, 3, 5. The values of 0.03, 0.3 and 3 has been chosen considering the pioneering work of Sassen and Cho (1992), who defined these thresholds to define sub-visible, thin and opaque cirrus clouds. A winter and two summer cases has been simulated, whereby 0.5 cm and 1.2 cm are the average seasonal values, and 1.5 cm is used to assess the sensitivity of IBT and DLI to larger column water vapor below the cloud.

The increase in the value of DLI and IBT as a function of the cirrus optical thickness is presented in Figure S3 for both the winter and summer case. The labels close to the lines show the increase in the value of DLI and IBT compared to that of the clear sky simulation.

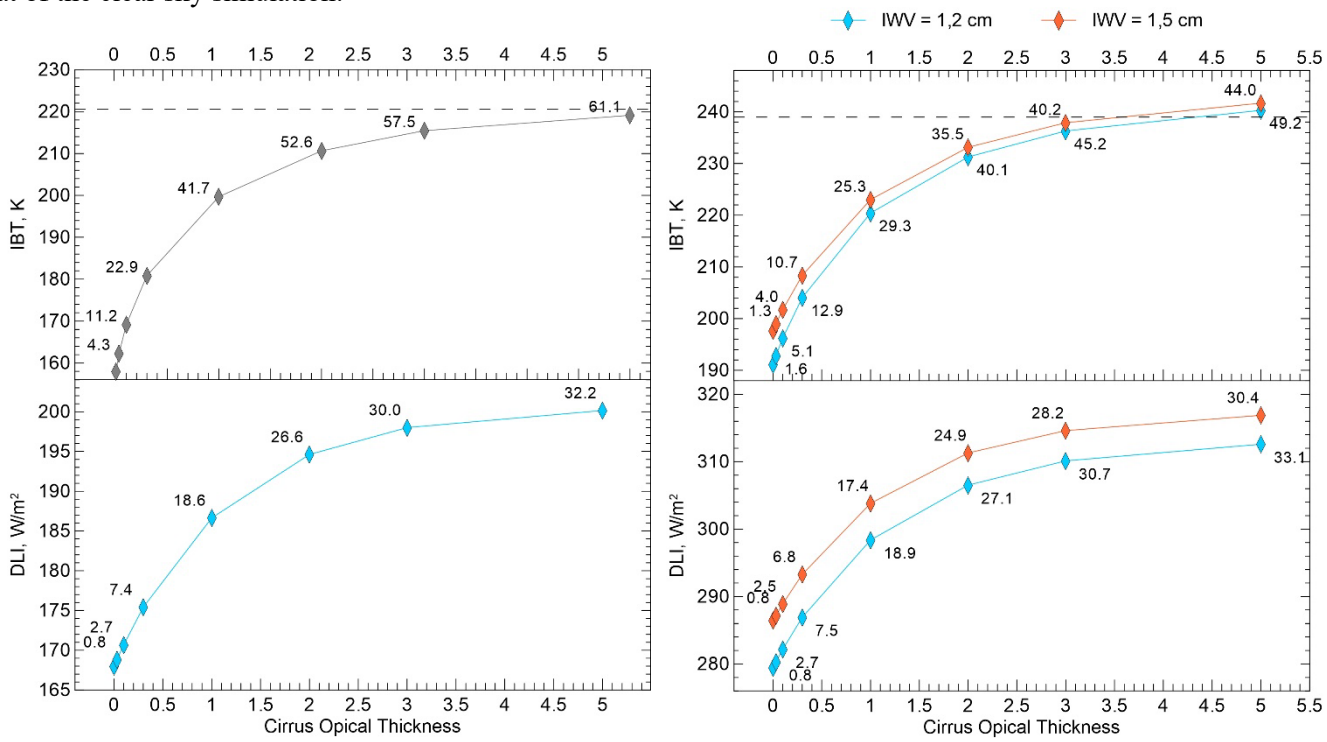

Figure S3. The plots show the DLI (in the bottom panel) and the IBT (in the top panel) increase as the optical thickness of the cirrus cloud increases, for the winter (left) and the summer (right) case respectively. The labels show the increase in the value of DLI and IBT compared to that of the simulation in the absence of cirrus. A horizontal dotted line highlights the temperature of the cloud base in the winter and summer cases.

The clear-sky IBT for the winter case is 158 K, which is below the pyrometer's calibration range, i.e. down to 173 K, but within its measurement range, i.e. down to 123 K. Even the presence of cirrus with optical thicknesses of 0.03 and 0.1 determines an increase in the pyrometer signal of 4.3 and 11.3 K, respectively equal to an increase in IBT of 2.7% and 7.1%, respectively, compared to cloud-free conditions. Both these values are clearly visible compared to the background signal and within the pyrometer measurement uncertainty that, considering the temperature at the base of the cirrus, is approximately ±1.6/2.0 K. On the other hand, the increase in DLI with respect to its cloud-free value (i.e. 168 W/m^2) is just 0.8 (0.5%) and 2.7 (1.6%) W/m^2, that is particularly small also taking in to account the uncertainty on DLI measurements that are estimated to be ±5 W/m^2.

Similar results are found for the summer simulations. In this case, two simulations were performed taking into account different values of IWV. For IWV equal to 1.2 cm, even considering cirrus optical thickness of just of 0.03 and 0.1 the IBT increases, compared to that with clear sky (i.e. 191.1K), by 1.6 (0.86 %) and 5.0 (2.66%) K, respectively. It should be kept in mind (see paragraph *2 Site and measurement* of the manuscript) that, by decreasing the temperature difference between the cloud base and the pyrometer, the IBT associate uncertainly (±1.3 K) decreases. The same cirrus cloud determine an increase in the clear skies value of DLI, i.e. 279.5 W/m^2, respectively of 0.8 (0.3%) and 2.7 (0.97%) W/m^2 for 0.03 and 0.1 optical depth. Further increasing in the IWV does not substantially change the results, although the decrease of the IBT sensitivity to this cirrus is larger than that of DLI.

In summary, the simulations highlight the larger sensitivity to the presence of thin clouds of the pyrometer compared to the pyrgeometer, especially in the polar environment characterized by low IWV and therefore larger transparency in the atmospheric window around 10 μm.
However, our method for defining clear skies is based more on the variability of the signal than on its intensity.
These simulations highlight how the better sensitivity of the pyrometer induces a larger variability of the signal which is therefore more suitable than that of the pyrgeometer to be used to define clear sky conditions, also because it is much less influenced by the IWV changes (see Figure S4).

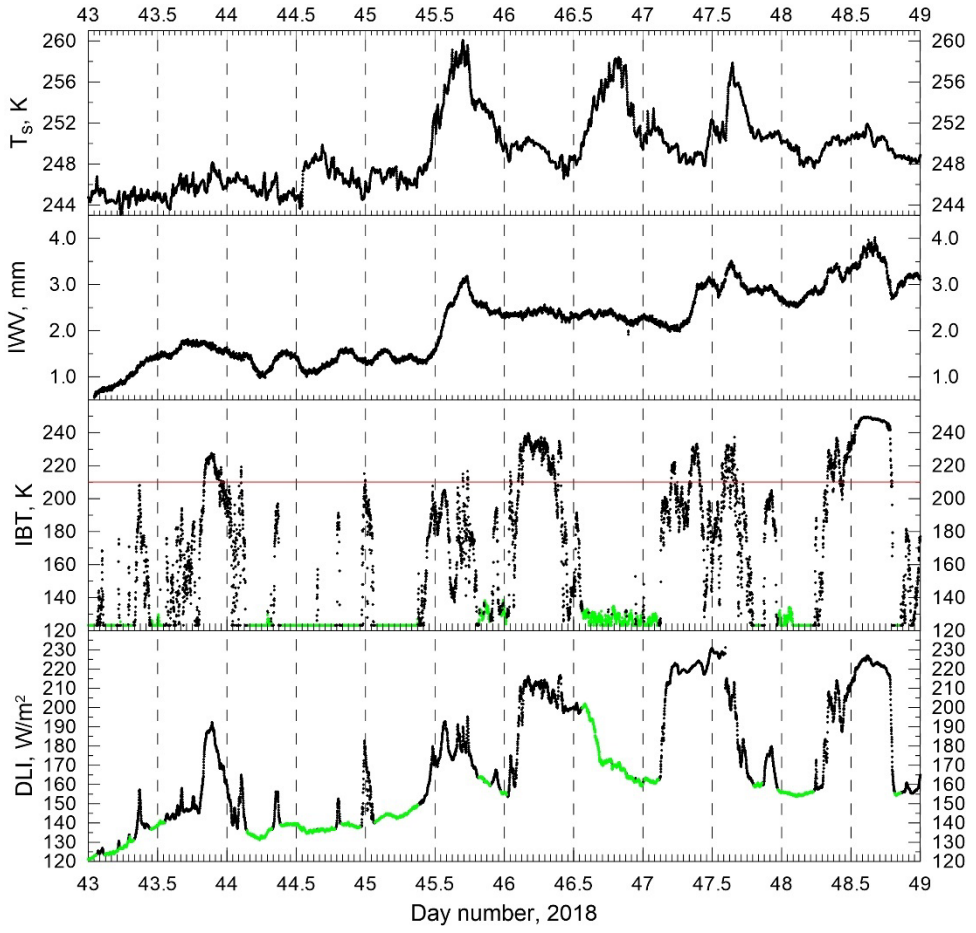

Figure S4. From bottom to the top: time series of DLI, IBT, IWV and Ts for the period from day number 43 to 49 of 2018, i.e. 12-18 February. As expected, the behavior of DLI is strongly dependent by the variability of IWV and Ts, which do not always show similar patterns.

Furthermore, it must be considered that zenith measurements are generally more sensitive to the 2D spatial variability of the cloud than hemispheric measurements. It is therefore unlikely that the algorithm can indicate a *zenith clear sky case* condition corresponding to the presence of a cloud that significantly influences the DLI.

Considering the results of the simulations and the visual inspection of the data (e.g. Figure S4 and discussion in the following), using a conservative approach, the methodology correctly evaluates the presence of cirrus clouds with an optical thickness larger than approximately 0.07-0.1 that, depending by the atmospheric profile (mostly IWV), and the physical (cloud base height, geometric thickness) and microphysical characteristics (ice content, size, shape...) of cirrus should determine an increase in the IBT value of no less than 7/15 K.

Considering the interest that both reviewers have shown in the clear sky algorithm and to better answer their questions, we present and discuss an example of how the algorithm operates to recognize clear sky cases, or perhaps it would be better to say cases where the presence of clouds does not appreciably influence the DLI.
Figure S4 shows six days of IBT, DLI, IWV and T_s measurements collected in February 2018; cases recognized as clear sky are shown as green points.

The algorithm proves to have enough sensitivity to detect very thin clouds that only slightly increase DLI, but determine a IBT increase of approximately 15 K or less (e.g., see the IBT on the beginning of day 43). Although the algorithm proves to work well in relation to the purpose of this analysis, we have chosen to present this case to highlight what has already been mentioned in manuscript lines 167-175, i.e. the importance of visual control of the clear sky.
In the time interval from 46.55 to 46.7 the IBT does not highlight any clouds, while the DLI shows a decrease suggesting residual coverage of the sky. Although this hypothesis cannot be discarded, observation of the sky images shown in Figure S5 suggests another explanation.

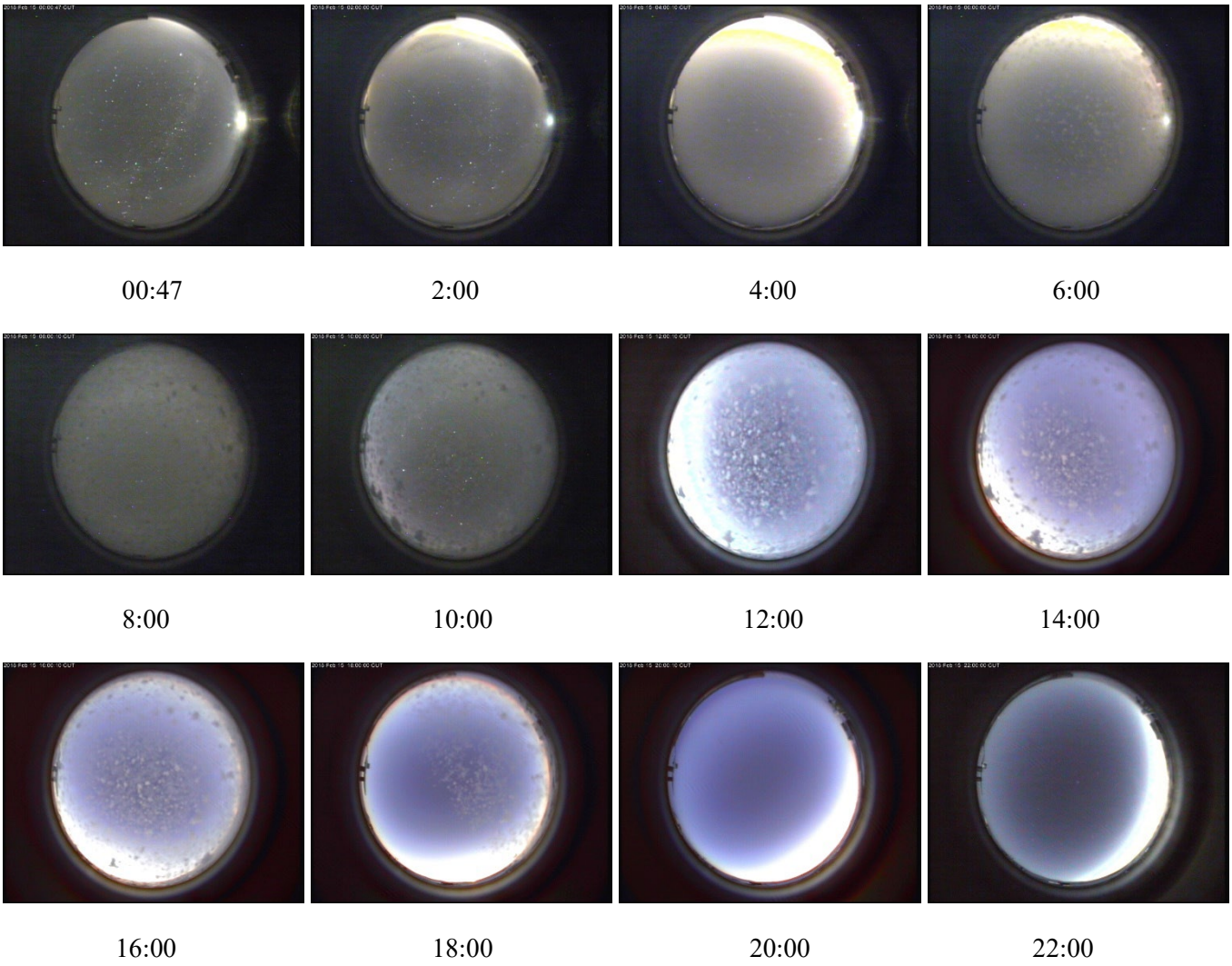

Figure S5. Bi-hourly sky images of day 46 of 2018 (15 February 2018).

Just as happened on the dome of the sky imager between 6 and 18, it is probable that some frost condensed on the dome of the pyrgeometer and then slowly sublimated. This can occasionally occur even if the pyrgeometer is ventilated. In addition, the BSRN quality tests on DLI may not detect such effect. It should be remembered here that the surface of the window of the pyrometer is ventilated with an air flow coming from inside the observatory and is therefore less subject to these phenomena.
These phenomena and the presence of snowfall were the main obstacle to the correct and automatic functioning of the algorithm. Thanks to a visual analysis of the entire dataset their impact is considered negligible.

Also taking into account these effects it is much more complex to quantitatively demonstrate that the passage from a *zenith clear sky case* condition to a *clear sky*, i.e. hemispheric clear sky, does not include the residual presence of clouds. The choice to consider a relatively long series of *zenith clear sky cases* to define a *clear sky* condition (please remember that our method identifies a clear sky condition, e.g., at 12:00 if on the 61 IBT measurements ranging from 11:30 to 12.30 at least 45 zenith clear sky cases occur) is based both on the visual analysis of the dataset and the conclusion of two interesting articles, that by Kassianov et al. (2004) who states ”for a relatively short averaging time (15 min), the zenith-pointing observations with a narrow FOV (lidar/radar) can greatly (more than 100%) overestimate/underestimate the cloud fraction” and that of Dupont et al. (2008) who for comparing clear sky values derived from shortwave and longwave measurements with those derived from lidar measurements, used hourly lidar averages.

The choice to define a clear sky measurement by evaluating 61 *zenith clear sky measurements* was maybe a little bit conservative, but (also taking into account the large dataset used) it was preferred to remove some clear sky data rather than include dubious data.

Reference

Berk, A., Anderson, G. P., Acharya, P. K., Bernstein, L. S., Muratov, L., Lee, J., Fox, M., Adler-Golden, S. M., Chetwynd, J. H., Hoke, M. L., Lockwood, R. B., Gardner, J. A., Cooley, T. W., Borel, C. C., Lewis, P. E., and Shettle, E. P.: MODTRAN5: 2006 Update, Proc. SPIE 6233, https://doi.org/10.1117/12.665077, 2006.

Dupont, J.-C., M. Haeffelin, and Long, C. N.: Evaluation of cloudless-sky periods detected by shortwave and longwave algorithms using lidar measurements, Geophys. Res. Lett., 35, L10815, doi:10.1029/2008GL033658, 2008.

Kassianov, E., C. N. Long, and Ovtchinnikov M.: Cloud Sky Cover versus Cloud Fraction: Whole-Sky Simulations and Observations. J. Appl. Meteor. Climatol., 44, 86–98, https://doi.org/10.1175/JAM-2184.1, 2005.

Sassen, K., and Cho B. S.: Subvisual-Thin Cirrus Lidar Dataset for Satellite Verification and Climatological Research. J. Appl. Meteor. Climatol., 31, 1275–1285, https://doi.org/10.1175/1520-0450(1992)031<1275:STCLDF>2.0.CO;2, 1992.